Available online at www.sciencedirect.com
SCIENCE DIRECT®
ELSEVIER
Journal of Magnetism and Magnetic Materials 266 (2003) 215–226
journal of magnetism and magnetic materials
www.elsevier.com/locate/jmmm

Crystallographic ordering studies of FePt nanoparticles by HREM

Mihaela Tanase[a,*], Noel T. Nuhfer[a], David E. Laughlin[a], Timothy J. Klemmer[b], Chao Liu[b], Nisha Shukla[b], Xiaowei Wu[b], Dieter Weller[b]

[a] *Data Storage Systems Center, Carnegie Mellon University, 5000 Forbes Avenue, Pittsburgh, PA 15213, USA*
[b] *Seagate Research, Pittsburgh, PA 15222, USA*

Received 21 November 2002; received in revised form 24 March 2003

Abstract

FePt nanoparticles with a size of 4 nm were prepared by the polyol process according to the reaction route described by Sun et al. The particles were annealed at 550°C and 580°C for 30 min in N_2 atmosphere, developing coercivities of up to 8.8 kOe. From conventional transmission electron microscopy the coherence lengths of the self-assembly were found to be as large as 10 μm in the as-prepared state and about 1 μm in the annealed state. The degree of sintering is zero for the 550°C annealed samples and only a small amount for the 580°C annealed samples. Ordering of the as-prepared fcc structure of the FePt nanoparticles into the $L1_0$ structure as a result of annealing is studied by high-resolution electron microscopy. In this investigation monodispersed nanoparticles are frequently found to undergo partial chemical ordering to the hard magnetic $L1_0$ phase without a change in size. Qualitative HREM observations about the amount of ordering of monodispersed nanoparticles, the low degree of sintering of the samples and large coherence length of the self-assembly together with the high coercivity developed upon annealing suggest the potential production of self-assembled ferromagnetic FePt arrays in future high-density magnetic data storage.

Keywords: FePt; Nanoparticles; Self-assembly; L10; Ultra-high density recording media

1. Introduction

The interest raised by nanoparticle materials as a new generation of advanced materials is justified by their size-dependent properties which open wide research areas in most fields of engineering of nanophase materials and devices [1]. In magnetic data storage, the application of metallic nanoparticles as a data storage medium is being intensely pursued, and among these, $L1_0$ FePt nanoparticles are the most promising due to the high value of their magnetocrystalline anisotropy (6.6×10^7–10^8 erg/cm^3). This together with size distributions as narrow as 5% [2] makes them a good candidate in the pursuit of scaling down the bit cell surface area by reducing the grain count per bit.

Sun et al. [2] have shown that high-coercivity self-assembled lattices of FePt nanoparticles can be prepared using the polyol route and subsequent thermal annealing. However, the main problem

*Corresponding author.
E-mail address: mtanase@andrew.cmu.edu (M. Tanase).

0304-8853/$ - see front matter © 2003 Elsevier B.V. All rights reserved.
doi:10.1016/S0304-8853(03)00480-3

faced by this procedure is the large-scale decay of the self-assembly due to heating, which is needed to induce the phase transformation of the fcc particles to the high-anisotropy $L1_0$ phase. Annealing at low temperatures gives low diffusion mobility which slows down the chemical ordering, whereas at high temperatures the high diffusion mobility favors the transformation, but allows for the possibility of sintering and other annealing phenomena. At this stage of our research in the preparation and post-annealing of FePt arrays the optimal temperature range is 450–650°C. However, a compromise is needed between the high driving force for ordering, suitable diffusion and prevention of the decay of the self-assembly.

Moreover, the processes that occur in FePt nanoparticle samples as seen in conventional transmission electron microscopy and in HREM are far from being homogeneous across the surface. On a sample which exhibits some degree of sintering at a given location, the phenomena associated with earlier and later stages of the sintering process occur at other locations as well. These phenomena include: distortion of the self-assembly, agglomeration of nanoparticles and grain growth.

For definition purposes, we understand by distortion of the self-assembly the loss of long-range periodicity of the nanoparticles. Agglomeration represents the physical migration of nanoparticles on the substrate so as to come in contact with other particles without an exchange of atoms by diffusion and without changes in the crystalline structure. Sintering occurs when particles in contact begin exchanging atoms so that the distance between their centres becomes less than the sum of their initial radii. Grain growth involves the movement of a grain boundary across a pre-existing particle boundary and may or may not be accompanied by chemical ordering.

A systematic quantitative study of these phenomena occurring in FePt nanoparticles as a function of the annealing conditions has not been published yet. In this paper, we report our initial studies of the changes in the microstructure due to annealing that occur both locally and globally and we associate these changes with the corresponding sintering stages. Assessment of the amount of sintering on a macroscale as well as of its physical location on the grid is made possible by the one-to-one correspondence between the different microstructures and their appearance in low magnification. Understanding these thermally activated processes and the role of the substrate in the heating process will eventually enable the control of chemical ordering in the nanoparticulate FePt system.

Recently, a theoretical comparison of the relative driving forces for chemical ordering and other solid-state reactions as well as the consequences of combined reactions has been presented [3]. Although the combined reactions mechanism of sintering, ordering and/or grain growth is energetically favoured, there is no principial constraint imposed on the ordering of lone nanoparticles without loss of monodispersity. Therefore, there are a number of questions that arise, all pertaining to the quantitative side of the problem: How much sintering occurs at a given point in the time–temperature space? What is the ratio of monodispersed versus sintered nanoparticles which have undergone the phase transformation? What is the relative contribution of monodispersed versus sintered nanoparticles to the coercivity? We are proposing to address these issues in a semi-quantitative manner and emphasize the occurrence of chemical ordering in monodispersed nanoparticles in the context of other annealing effects.

2. Experimental methods

Four-nanometer FePt nanoparticles are prepared by the reaction route described by Sun et al. [2] and optimized for obtaining a stoichiometric composition. Samples are washed according to Sun et al. [2] and deposited on SiO_2-coated copper grids by evaporation from solution. They are annealed in flowing N_2 atmosphere in a rapid thermal annealer at 550°C and 580°C for 30 min. The HREM studies are carried out using a Philips TECNAI F20 TEM/STEM/GIF microscope with an operating voltage of 200 kV and a point resolution of 2.4 Å. Conventional transmission electron microscopy studies were carried out using

a Philips EM420T microscope operating at 120 kV, with a point resolution of 3.5 Å. Magnetic measurements are carried out at room temperature using superconducting quantum interference device magnetometry.

3. TEM experimental results and discussion

Figs. 1(a) and (b) show TEM images in low and high magnification, respectively, of a sample in the as-prepared state consisting of disordered fcc nanoparticles. Fig. 1(a) shows the image of a 300 mesh grid slot, where the dark contrast regions are areas of assembled nanoparticles and the light contrast regions are bare substrate. The coherence length of the assembly is typically 10 μm along the edge of the grid slot. Fig. 1(b) represents the self-assembly at the nanoscale showing six-fold symmetry. As seen from Fig. 1(a) the grid coverage is about 22%. An image of a nanoparticle as obtained from the preparation procedure is shown in Fig. 1(c). Nanoparticles have truncated octahedron shapes with (1 1 1), (2 2 0) and (1 0 0) facets, which are smooth or can exhibit (1 1 1) atomic steps as in Fig. 1(c). The surface structure and faceting of these nanoparticles have been described elsewhere in detail [1,4,8].

By changing the washing procedure the nanoparticles can be obtained in assembled multilayers with a comparable coherence length. Fig. 2(a) shows a 100% covered sample in low magnification (grid edges are visible in the lower part of the image for visual guidance). The area shown is enlarged in Fig. 2(b) and displays 'islands' of assembled material of different thicknesses. Further enlargement (Figs. 2(c) and (d)) reveals the structure and thickness of the 'islands'. They

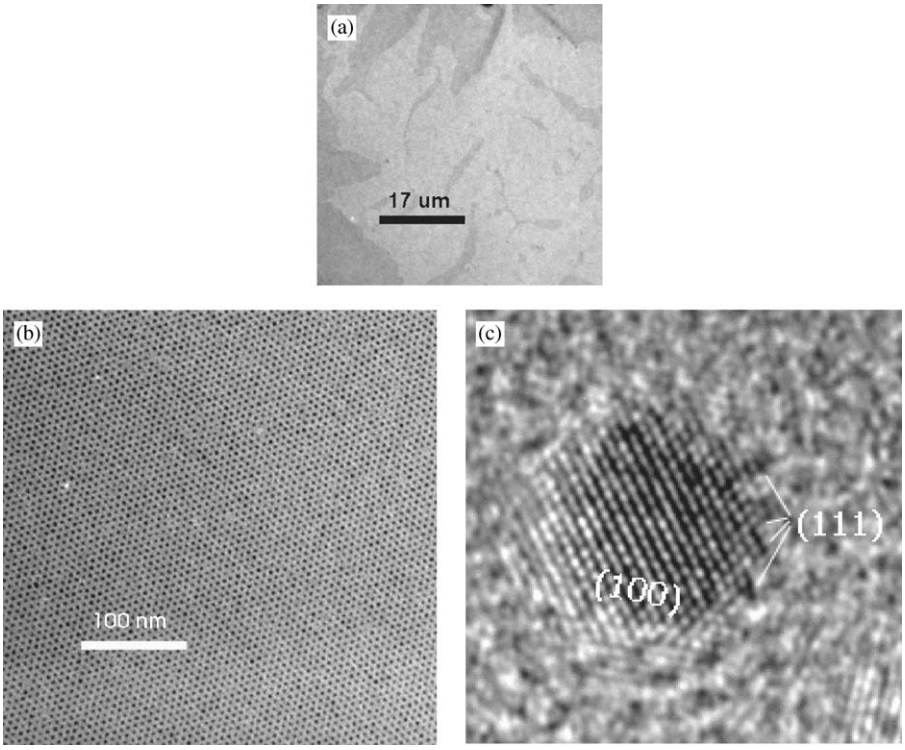

Fig. 1. (a) Low-magnification view of one slot of the TEM grid; material coverage is about 22%; covered area (dark grey contrast) consists entirely of assembled monolayers with a coherence length of 10 μm; light-contrast area is the bare supporting film. (b) High-magnification view of the assembled monolayer shown in (a). (c) Structure of a single FCC nanoparticle as composing the six-fold assembly shown in (b), showing (1 1 1) atomic steps on the surface.

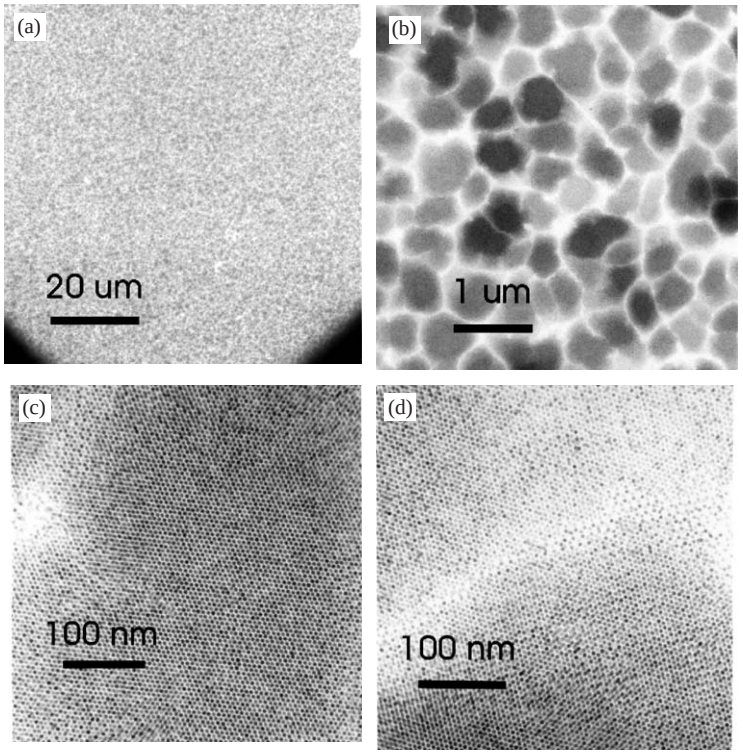

Fig. 2. (a) Low-magnification view of grid, showing uniform coverage at a macroscale. (b) Enlarged view of (a) showing the layer thickness variation forming 'islands' of nanoparticles. (c) Enlarged view of (b); number of nanoparticle layers varies from 1 to 6, visible by contrast; layers follow the ABC stacking characteristic of the assembly. (d) Nanoscale view of the transition region between two thickness 'islands'; transition layer has the same orientation and periodicity as the neighbouring regions, therefore thickness 'islands' are coherent among them; coherence length is 3–4 μm, extending across several of these islands.

are stacked assembled layers ranging in thickness from 1 to 5–6 nanoparticles (visible by contrast, see Fig. 2(c)), connected by coherently assembled monolayers. Despite the thickness variation, the coherence length typically extends over 3–4 μm, across several of these 'islands'. An enlarged view of the coherent transition between two neighbouring 'islands' is shown in Fig. 2(d).

In the case of the annealed samples the coherence length is up to 1 μm. Fig. 3(a) shows a low-magnification image of one of the grid slots of a sample annealed at 580°C/30 min, in which different contrast regions uniquely correspond to specific microstructures. Fig. 3(b) shows an enlarged view of the edge of the grid slot, in which the dark contrast marked with 'A' represents assembled multilayers (see enlarged in Fig. 3(c)) and the medium contrast (marked with 'B') represents a mixture of assembled bi/trilayers and a disordered monolayer (see enlarged in Fig. 3(d)). The region marked with C is a disordered monolayer which covers most of the surface of the sample and can be seen enlarged in Fig. 3(e). The features marked 'D' are sintered regions and are shown at the nanoscale in Fig. 3(f). The individual nanoparticles can be seen to be either monodispersed around the sintered region or coalesced within it. A sintered region is composed of partially sintered nanoparticles, which may still have spaces in between their contact points. Assembled multilayers are located along the grid edges, just as in the case of the as-prepared samples with a typical coherence length of 1 μm. The sintering process implies the physical migration of particles on the substrate (agglomeration) and exchange of atoms between neighbouring

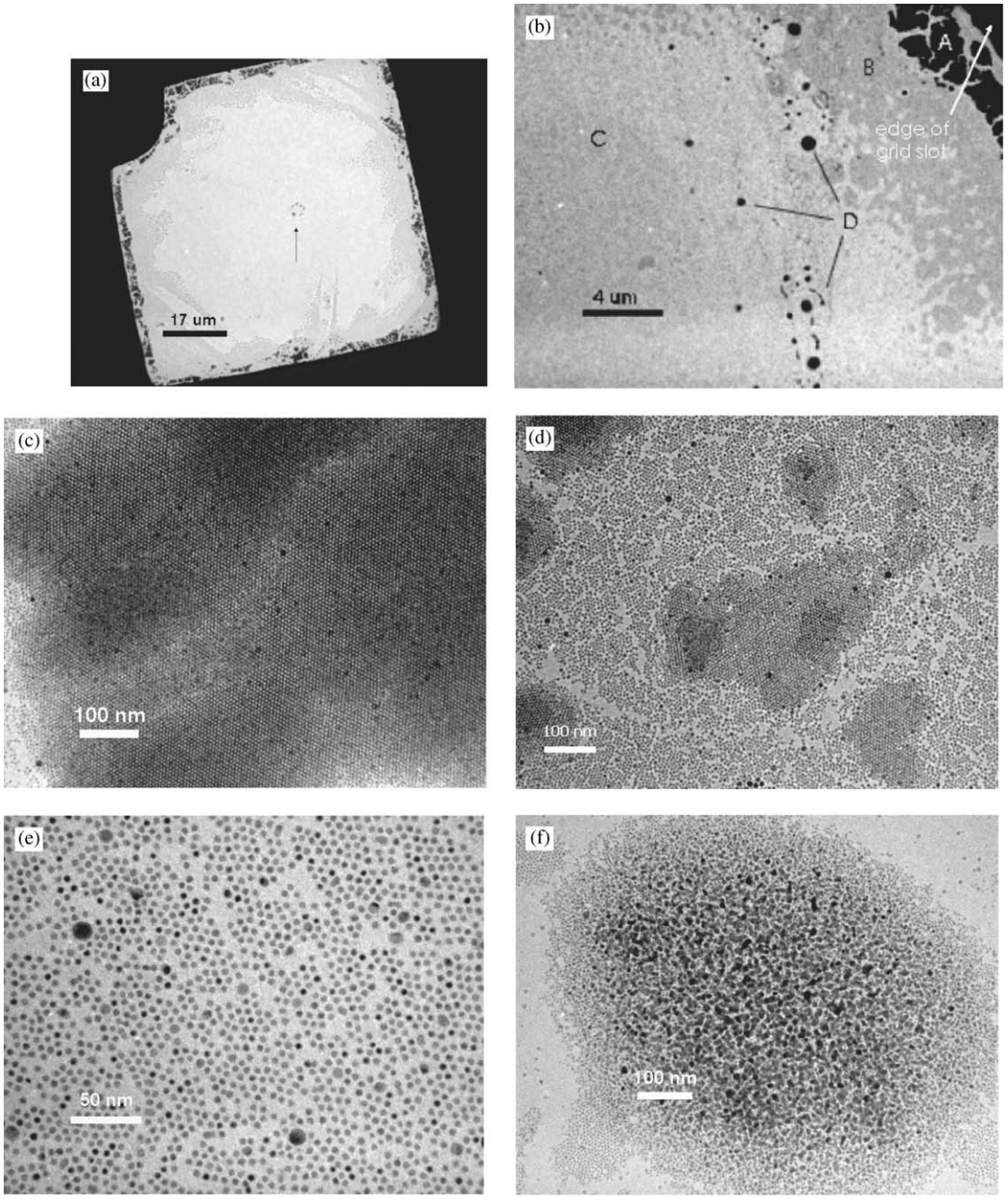

Fig. 3. The 580°C/30 min anneal. (a) Low-magnification view of a grid slot; the occurring features and their contrast are described in (b)–(f). (b) an enlarged view of the edge of the grid slot: (i) the dark contrast marked with 'A' represents assembled multilayers; an enlargement of an 'A' region is shown in (c); (ii) the medium contrast marked with 'B' represents a mixture of assembled bi/trilayers and a disordered monolayer; an enlargement of 'B' is shown in (d); (iii) the features marked 'D' are sintered regions (see Fig. 3(f) for an enlargement showing individual nanoparticles coalesced in one of these sintered regions). (c) Self-assembled multilayer. (d) Self-assembled bi/trilayer and disordered monolayer. (e) Disordered monolayer makes up for most of the sample; sintered particles of larger size can be observed among the monodispersed nanoparticles. (f) A sintered region in which individual nanoparticles can be observed in monodispersed state towards the edges of the picture and coalesced in the middle of it; sintering is not complete since there are voids visible in between particles.

nanoparticles and eventually complete coalescence. It appears that nanoparticles are more likely to stay self-assembled upon annealing when their number of degrees of freedom are reduced, as for example when they are stacked in multilayers and/or due to the confinement provided by the substrate irregularities or by the grid edges. Fig. 3(d) illustrates one type of confinement present (multilayering) when the thermal energy transferred to the particles due to the heating breaks up the assembly into islands, reducing the coherence length of the structure typically to 100 nm. Grid edge confinement combined with multilayering results in a good coherence length of about 1 μm, as can be seen in Fig. 3(c). However, multilayering brings about the unwanted effect of atomic exchange between nanoparticles even if the self-assembly is not distorted yet. Away from the edges of the grid (lightest contrast in Fig. 3(a), enlarged in Fig. 3(e)) an initially assembled monolayer is distorted by the thermal energy and the nanoparticles have rearranged. Statistical analysis of the distribution of the X–Y coordinates shows that particles tend to re-arrange so as to increase the mean interparticle spacing, therefore the distorted monolayer covers a larger area than before annealing. This is possible because the initial grid coverage is about 22%, the rest of the substrate being bare. Size distribution analysis gives a 4 nm average size for the unannealed nanoparticles, the effect of the annealing being a broadening of the size distribution. It can be seen from Fig. 3(e) that a small percentage of the particles are already sintered. There are two types of sintering which can be identified as: (1) sintered nanoparticles of up to 13 nm diameter found randomly on the entire area of the sample (as seen in Figs. 3(c)–(e)) and (2) large sintered regions of typically 1 μm in size made up of tens of thousands of coalesced nanoparticles (as seen in Fig. 3(f)). The most striking difference between types 1 and 2 of sintering besides their difference in size is their location: sintered nanoparticles can be encountered throughout the viewing area regardless of the presence of the assembled regions, whereas sintered regions are found only among the disordered monolayers, away from the grid edges and are easily recognized by shape and contrast in low magnification (see arrow in Fig. 3(a) and region D in Fig. 3(b)). The area covered by sintered regions accounts for less than 2% of the viewable surface. Moreover, this type of sintering only appears after thermal treatments above 550°C while the first type develops gradually with temperature. The morphology of the 550°C 30 min annealed sample is identical with the one of the 580°C/30 min described here, the only difference being the lack of sintering of the second type.

4. HREM experimental results and discussion

The HREM study focuses on the structure of individual monodispersed nanoparticles and the crystallographic changes that result from thermal annealing. The purpose of this study is to answer the question whether the coercivity in the annealed samples is due entirely to the sintered nanoparticles, or if monodispersed nanoparticles also contribute to it. The approach is a statistical one: through random imaging on the sample we counted the number of occurrences of monodispersed nanoparticles which exhibit some degree of chemical order. We have frequently found evidence of ordering within monodispersed nanoparticles in both monolayers (Fig. 4(a)) and multilayers (Fig. 5(a)). We note that the number of ordered nanoparticles is even larger than the number observed because not all ordered particles have the suitable zone-axis orientation for imaging (with the c-axis in the plane of observation). In multilayers, evidence of ordering is even more difficult to find due to partial overlapping of lattice fringes belonging to adjacent and/or superposing particles. The quantification of the degree of ordering in nanoparticles should take into account both the order parameter (related to c/a ratio) and the size of the ordered region within the particle. Fig. 5(b) shows an enlargement of the ordered particle from Fig. 5(a) and shows a combination of c/2 spacing (lower left corner) and c spacing, which indicates that the size of the ordered region is smaller than the size of the particle. The fast Fourier transform of the nanoparticle in Fig. 5(b) is shown in Fig. 5(c) where the superlattice

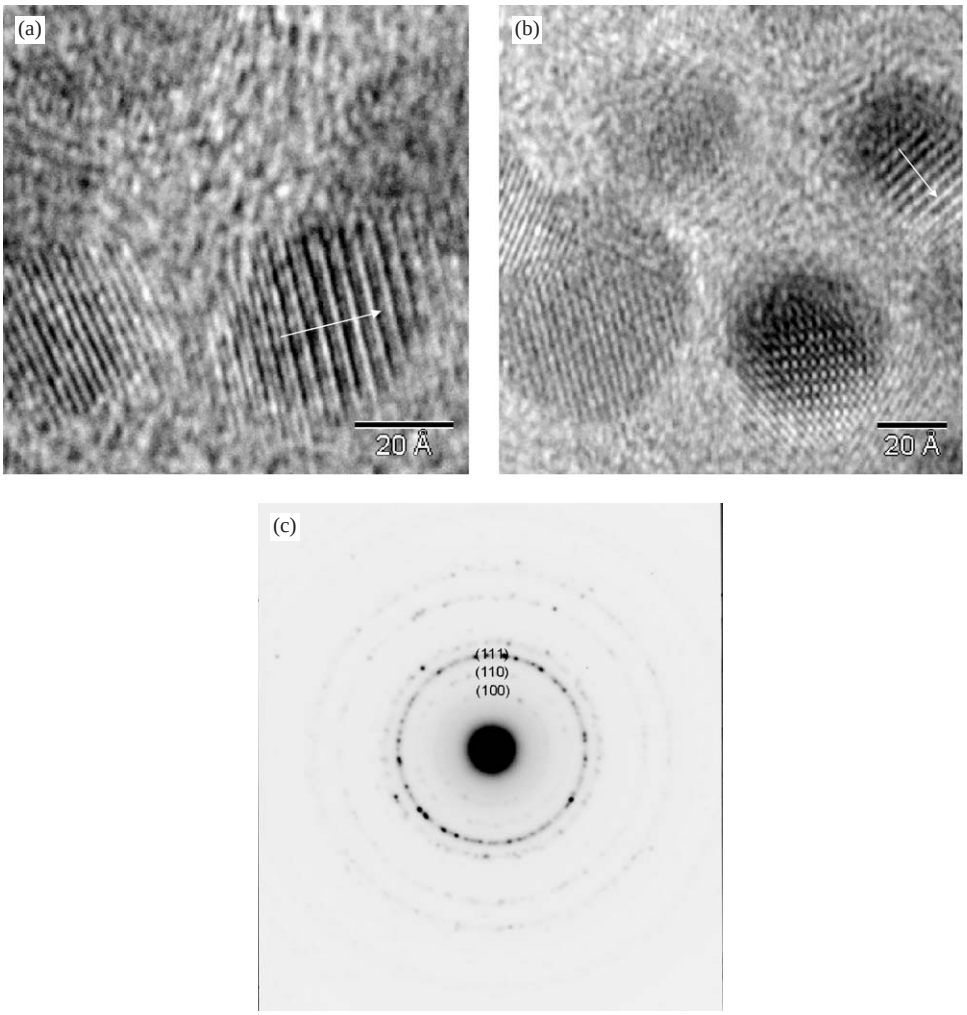

Fig. 4. (a) Monodispersed nanoparticles which upon annealing exhibit a partial transformation to the tetragonal $L1_0$ phase without a change in size; white arrows indicate the *c*-axis lying in the plane of observation. (b) Electron diffraction pattern of an annealed sample showing development of the $L1_0$ phase.

reflections (0 0 1) can be clearly seen. The electron diffraction pattern of a 580°C 30 min annealed sample is shown in Fig. 4(b).

The beginning of the sintering process can be seen in Fig. 6(a). Two particles have agglomerated and their relative orientation is arbitrary. Each nanoparticle is near a zone axis, displaying only one set of fringes. The angle between the two sets of lattice fringes is 75.5°. The lattice periodicities are (2 0 0) for the upper particle and (1 1 1) for the lower particle so a twin structure is excluded. Fig. 6(b) shows the aggregation of two nanoparticles with the formation of a low-angle boundary. The orientation is close to [1 1 0]. While the right particle is almost perfectl in zone axis, the left one exhibits a single set of (1 1 1) planes and the region of fringe intersection comprises all three pairs of reflections.

An example of a coherent boundary is shown in Fig. 7(a). In the lower part of the picture two aggregating nanoparticles can be seen. From the FFT image (Fig. 7(b)) the angle between lattice fringes is 110.2°. Lattice fringes on both sides of the defect line have periodicity of $a/\sqrt{2}$ which

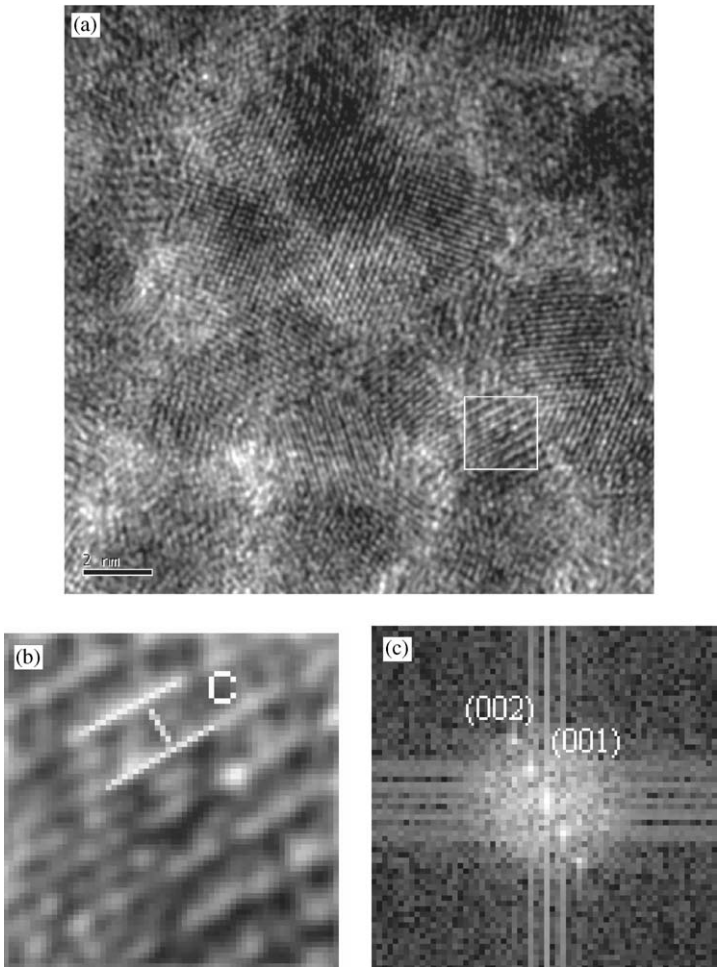

Fig. 5. (a) Assembled nanoparticle bilayer (six-fold pattern visible) with one nanoparticle exhibiting chemical ordering. (b) The ordered nanoparticle from (a); ordering is not complete as can be seen from the presence of single and double c/2 spacing. (c) Fast Fourier Transform of (b) showing the superlattice reflections (0 0 1) indicative of chemical ordering.

indicates {1 1 0} planes. The reconstruction of the image using the FFT filtering technique (not displayed here) shows that the fringes belonging to different pairs of reflections do not overlap spatially in the reconstructed image. This rules out the possibility of a single zone axis since the two (1 1 0) reflections come from spatially distinct regions. The defect in this case is identified to be a (1 1 1) twin. The simulated (1 1 1) twin in the hypothesis of an ordered structure is shown in Fig. 7(c). It is still unclear here whether the (1 1 1) twin forms within the lower particle itself or develops during the sintering process. However, this type of twin has frequently been observed in annealed FePt nanoparticles.

Sintered nanoparticles exhibit order in HREM less frequently which is attributed to their polycrystallinity. This poses the same visualization problem as the ordering of monodispersed nanoparticles in multilayers. Sintered nanoparticles as seen in Fig. 3(e) are studied in HREM and are shown in Figs. 8(a) and (b). From Fig. 8(a) it can be seen that the lattice fringes belonging to the sintered particle have different directions and periodicities, which means the random agglomeration of the constituent nanoparticles during

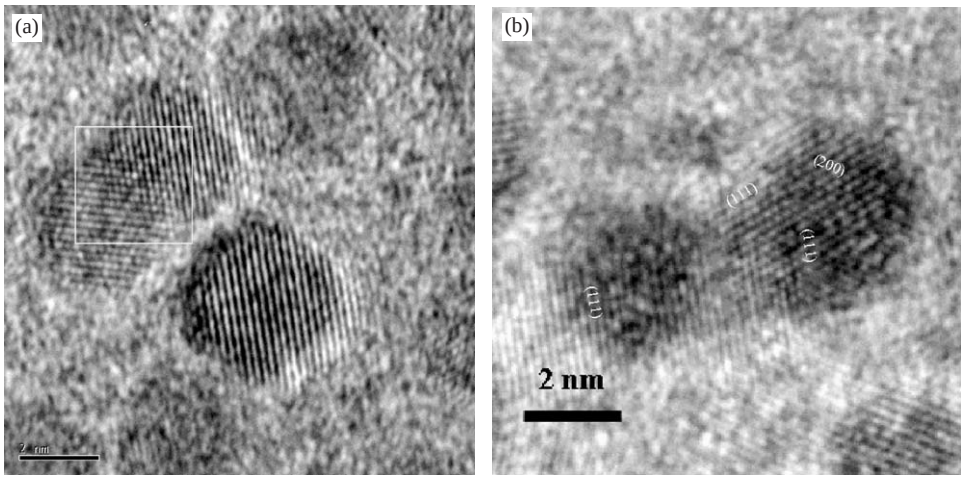

Fig. 6. Beginning of the sintering process—incoherent aggregation: formation of (a) a high-angle boundary and (b) a low-angle boundary.

sintering. Fig. 8(b) pictures a sintered nanoparticle with only one of the constituent nanoparticles oriented in zone axis.

A later stage of nanoparticle sintering is shown in Fig. 9(a). The larger particle has formed from several monodispersed nanoparticles which have completely coalesced into one grain exhibiting a high degree of chemical order. The direction of the *c*-axis and the alternating Fe and Pt layers can be seen in the [1 1 0] zone axis.

HREM data need to be correlated with other techniques in order to assess the amount of order on the samples. From SQUID measurements at room temperature, the coercivity of the 580°C/30 min sample consisting of thick layers of nanoparticles deposited onto Si substrate was found to be 8.8 kOe. Since coercivities larger than 8.8 kOe have been reported in FePt nanoparticles [5–7], this value may be the result of the very fine particle size and/or partial chemical ordering. Since the initial size of the monodispersed nanoparticles is larger than the superparamagnetic limit for fully ordered FePt (3.1 nm), many of the ordered monodispersed nanoparticles are also ferromagnetic.

Because a large portion of the nanoparticles deposited on the TEM grid are not sintered we suspect that the coercivity of the nanoparticles deposited on the Si substrate is primarily from partially ordered or fully ordered monodispersed particles. However, it is important to note that different nanoparticle formations may be present on a TEM grid when compared to an Si substrate, which could cause a different ordering and sintering kinetics. From TEM measurements the amount of surface sintering on the 580°C/30 min sample was evaluated at about 2%. This type of sintering develops above 550°C on SiO_2 substrates whereas type 1 sintering (isolated sintered nanoparticles with sizes around 13 nm) was observed at both temperatures. However, the frequent occurrence of order in monodispersed nanoparticles as seen in HREM and their dominance in the TEM sample suggests that they have a large contribution to the magnetic coercivity.

5. Conclusion

FePt nanoparticles with size of 4 nm were prepared by the polyol process according to the reaction route described by Sun et al. [2]. The particles were annealed at 550°C and 580°C for 30 min in N_2 atmosphere. Conventional TEM investigations show that unwanted processes during annealing like agglomeration, sintering and grain growth occur inhomogeneously across the

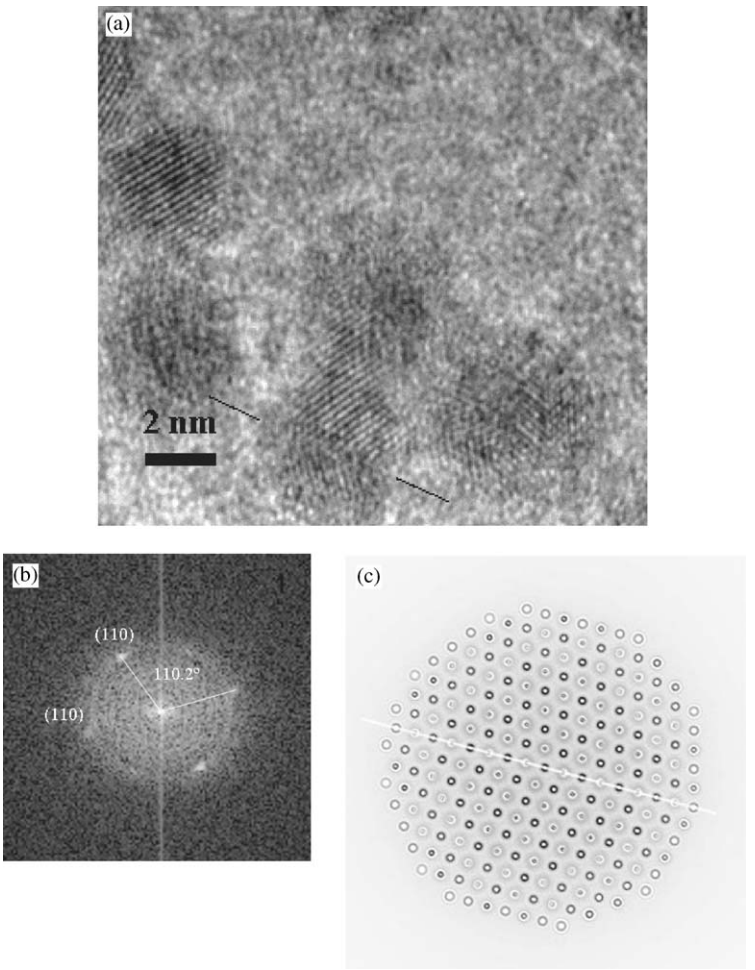

Fig. 7. Beginning of the sintering process—coherent aggregation: (a) a (1 1 1) twin, guidelines show the position of the twin plane; (b) FFT of twin shown in (a); (c) simulation of the (1 1 1) twin; white line indicates the intersection of the (1 1 1) twin plane with (1$\bar{1}$0) (the plane of view).

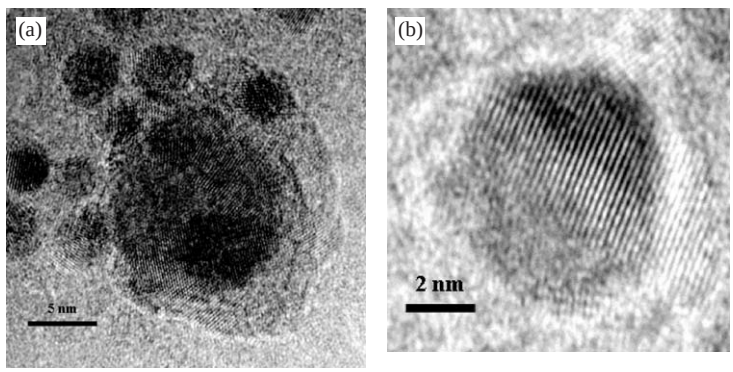

Fig. 8. Reflections from constituent particles are at arbitrary angles with respect to one another (sintered particles are generally polycrystalline): (a) several constituent particles are in zone axis and (b) a single constituent particle is in zone axis.

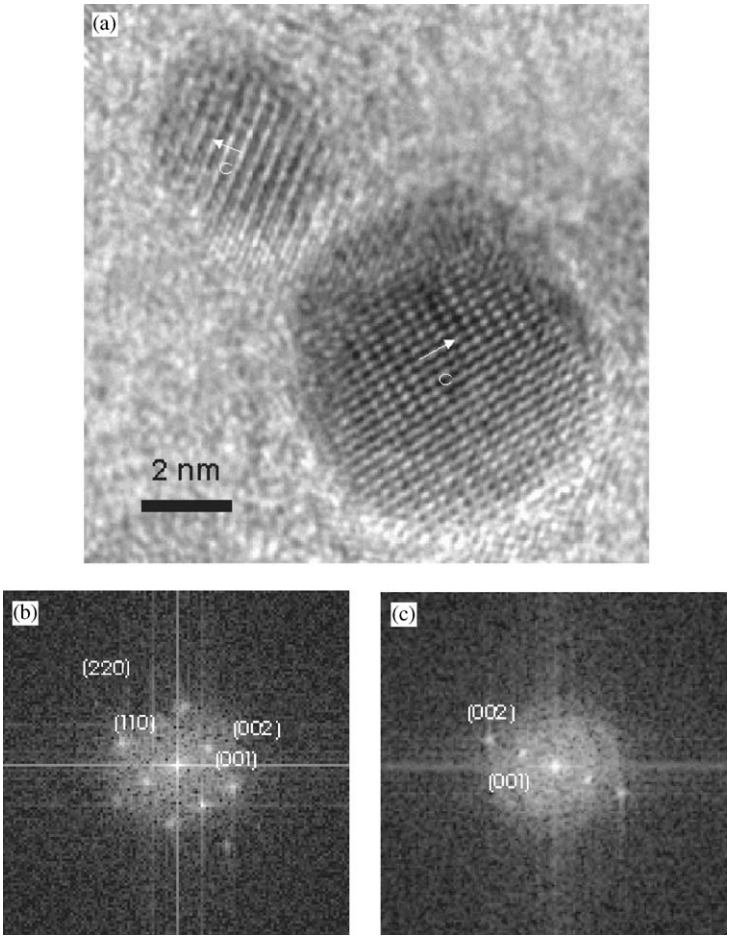

Fig. 9. (a) A sintered and a monodispersed nanoparticle, both ordered with the same periodicity;0 *c*-axis direction shown by white arrows. (b) Fast Fourier transform of the sintered nanoparticle shown in (a) showing the superlattice reflections (0 1 0) and (0 0 1). (c) Fast Fourier transform of the monodispersed nanoparticle shown in (a) showing the superlattice reflections (0 0 1).

surface of the sample. For the 580°C/30 min annealing conditions the self-assembly is preferentially preserved along the grid edges in multilayers with a thickness of 5–6 layers and a coherence length of 1 μm. Away from the grid edges the self-assembly is preserved in stacking structures of 2–3 layers with a 10 times lower coherence length (~100 nm). The decay of the self-assembly is complete in monolayers and HREM imaging indicates that sintering in all its stages occurs here: agglomeration (Fig. 8(a)) and sintering (Figs. 8(a) and (b)), grain growth with ordering (Fig. 9(a)). The overall degree of sintering of the type 2 introduced in the text (sintered regions as in Fig. 3(f)) on the 580°C/30 min annealed sample is 2% (surface percent) and this type of sintering does not overlap the self-assembly. This type of sintering does not occur on the 550°C/30 min annealed sample. Sintered nanoparticles as in Fig. 3(e) are present across the entire surface of the sample in both annealing conditions, however with a small probability of occurrence.

HREM investigations yield a direct proof of the phase transformation of monodispersed particles from fcc to the chemically ordered $L1_0$ phase as a consequence of annealing. After the

transformation to the thermodynamically stable $L1_0$ phase, a sample annealed at 580°C for 30 min exhibits a coercivity of 8.8 kOe when deposited on Si substrate. Faulted structures in the monodispersed nanoparticles are occasionally present, occurring in the annealed state rather than in the as-prepared state. A common fault encountered in the ordered nanoparticles is the (1 1 1) twin, which is often observed as resulting from annealing in fcc-type crystals.

As a result of annealing, a small percentage of sintered particles (type 1) are formed from previously monodispersed particles with random orientations with respect to each other. Atomic ordering of sintered particles cannot always be demonstrated in bright field HREM imaging due to the random orientation of constituent particles (polycrystallinity). However, since the percentage of sintered particles is small, it is worth emphasizing the large-scale occurrence of chemical ordering in the monodispersed nanoparticles and their potentially large contribution to the magnetic coercivity.

Acknowledgements

We would like to acknowledge Tadakhatsu Okhubo from the National Institute for Materials Science (NIMS) in Tsukuba, Japan for useful HREM image simulations.

References

[1] Z.R. Dai, S. Sun, Z.L. Wang, Shapes, multiple twins and surface structures of monodisperse FePt magnetic nanocrystals, Surf. Sci. 505 (2002) 325.
[2] S. Sun, C.B. Murray, D. Weller, L. Folks, A. Moser, Science 287 (2000) 289.
[3] T. Klemmer, C. Liu, N. Shukla, M. Tanase, D.E. Laughlin, D. Weller, J. Magn. Magn. Mater., 266 (2003) this issue.
[4] Z.R. Dai, S. Sun, Z.L. Wang, Nanoletters 1 (8) (2001) 443–447.
[5] T.J. Klemmer, N. Shukla, C. Liu, et al., Appl. Phys. Lett. 81 (12) (2002) 2220.
[6] T. Shima, K. Takanashi, Y.K. Takahashi, K. Hono, Appl. Phys. Lett. 81 (6) (2002) 1050–1052.
[7] K. Sato, B. Bian, T. Hanada, Y. Hirotsu, Scr. Mater. 44 (2001) 1389–1393.
[8] Z.L. Wang (Ed.), Characterization of Nanophase Materials, Wiley-VCH Verlag GMBH, New York, 2000, Chapter 3.